Screening the Reactivity of Pt_xRu_y and $Pt_xRu_yMo_z$ Catalysts toward the Hydrogen Oxidation Reaction with the Scanning Electrochemical Microscope

S. Jayaraman and A. C. Hillier*

Department of Chemical Engineering, University of Virginia, Charlottesville, Virginia 22904

Received: November 18, 2002; In Final Form: March 19, 2003

We report an application of the scanning electrochemical microscope that exploits its ability to spatially map the kinetics of heterogeneous electron-transfer reactions in order to perform screening measurements for combinatorial studies of electrooxidation catalysts. The ability to measure the activity of catalyst surfaces toward the hydrogen oxidation reaction via tip−sample feedback is used to characterize the activity of Pt_xRu_y and $Pt_xRu_yMo_z$ catalysts as a function of composition and electrode potential. Multielement band electrodes containing various compositions of Pt_xRu_y and $Pt_xRu_yMo_z$ deposits are created via pulsed electrochemical deposition onto patterned substrates. Catalyst compositions are verified through a combination of Auger electron spectroscopy and energy-dispersive X-ray spectroscopy. Activity toward the hydrogen oxidation reaction is probed in sulfuric acid solutions by using a scanning microelectrode tip placed in close proximity to the catalyst surfaces. The tip potential is held at a value where protons are reduced to hydrogen at a diffusion-limited rate. Tip-produced hydrogen is converted back to protons via oxidation at the catalyst surfaces. This leads to an increase in feedback current at the tip, whose magnitude directly reflects the substrate's rate constant for hydrogen oxidation. Monitoring the feedback response while scanning the microelectrode tip over catalyst samples of various compositions is used to deduce the onset of activity. The onset of hydrogen oxidation on these Pt_xRu_y and $Pt_xRu_yMo_z$ samples in the presence of an adsorbed monolayer of carbon monoxide is determined by performing screening studies as a function of electrode potential. The compositions with the lowest onset potentials are identified, and the results are compared with carbon monoxide stripping experiments.

Introduction

One of the barriers limiting the development of polymer electrolyte membrane fuel cells as a competitive alternative energy source is the inability of existing anode catalysts to oxidize fuels other than hydrogen at sufficient levels.[1−3] In particular, the presence of carbon monoxide in the fuel, which can exist either as a byproduct from upstream reforming or be formed as a partial oxidation product during the direct oxidation of liquid fuels, poses a significant problem for platinum-based catalysts. Carbon monoxide adsorbs strongly to active catalytic sites on platinum and decreases reactivity to unsuitable levels.[4,5] A considerable amount of effort has been expended on the development and characterization of anode catalysts with potentially higher poison tolerance. A number of studies on platinum-based alloys have focused on the addition of oxophilic metals such as ruthenium,[6−11] molybdenum,[12−14] tin,[15−17] osmium,[18,19] and others[20−22] that promote CO oxidation at lower potential. Although improved performance over pure platinum has been demonstrated for a number of these systems, necessary levels of performance are yet to be achieved.[7,23]

The search for improved fuel cell catalysts will ultimately involve the discovery of new catalyst compositions in addition to continued fundamental studies of these materials to elucidate the origins of enhanced activity. One of the barriers impeding the discovery of more active and poison-tolerant anode catalysts is the vast parameter space that must be sampled in order to thoroughly evaluate the range of composition and structure that forms the basis of the next generation catalysts. The multifunctional requirements of catalysts for the direct oxidation of hydrocarbons, which include the ability to activate C−H, C−O, and even C−C bonds, suggest that optimum performance will require multicomponent binary, ternary, or even quaternary catalysts.[24] Given the vast number of potential catalyst combinations available for study, the traditional mode of sequential preparation and testing of new catalyst formulations is an intractable approach to efficiently map out parameter space. Also, since it is not realistic to synthesize and test every possible catalyst composition, the possibility exists that one might miss discovering the "true" optimal composition.

Combinatorial methods pose great promise to efficiently identify candidate materials or sample vast regions of composition space for further exploration.[25,26] Since its introduction in the 1980s, the concept of combinatorial materials synthesis and high-throughput screening has been applied to a wide range of fields. Combinatorial methods have been exploited in systems that include drug discovery,[27−29] luminescent materials and phosphors,[30,31] homogeneous and heterogeneous catalysis,[26,28,29,32−37] surface chemistry,[38,39] hydrothermal synthesis,[40,41] and dielectric materials and superconductors.[42] An attractive feature of combinatorial methods is their ability to systematically study the performance of materials toward a property of interest (for example, luminescence and reaction rate) as a function of a relevant material or processing parameter.

Several groups have been pursuing combinatorial methods for synthesis and characterization of heterogeneous catalysts.[35,43−48] One of the major requirements for the successful application of combinatorial methods in heterogeneous catalysis is the availability of screening tools that provide chemical

* To whom correspondence should be addressed. E-mail: ach3p@virginia.edu.

10.1021/jp0274886 CCC: $25.00
Published on Web 05/10/2003

information as well as being highly parallel with the capability of high-throughput processing. A variety of techniques have been developed for high-throughput screening for combinatorial methods in catalysis. These include infrared thermography,[46,49] scanning mass spectrometry,[44,47,50−52] gas chromatography,[35] resonance enhanced multiphoton ionization,[53−55] Fourier transform infrared imaging,[36,56,57] pH-sensitive fluorescence indicator,[24,43] visual colorimetric assay,[58] and reactive dyes.[59,60] In electrochemical systems, the application of electrode arrays with individually addressable electrodes allows for quantitative measurement of individual reaction currents.[48] The ease of constructing microfabricated electrode arrays via traditional microelectronics processing steps has facilitated these studies. Product detection schemes have also been developed. A pH-sensitive optical screening method was employed to identify the onset of methanol oxidation through detection of proton evolution.[43] Although this is a rapid and parallel method, it suffers from limited spatial resolution and an inability to discriminate between partial and complete oxidation processes. In addition, quantitative information concerning reaction rates, reaction pathways, and interfacial chemistry are absent in this method. To address these limits, we recently presented a screening method that quantitatively detects protons at a surface using the scanning electrochemical microscope (SECM).[61,62]

This paper describes further efforts based upon reactivity imaging with the scanning electrochemical microscope to quantitatively screen combinatorial samples in liquid systems. We employ a tip reaction that uses the H^+/H_2 redox couple to measure the activity of a substrate toward the hydrogen oxidation reaction.[63−65] Application of this technique for the characterization of multicomponent electrooxidation catalysts is described. Multielement band samples containing both Pt_xRu_y and Pt_xRu_y-Mo_z electrodeposited catalysts are interrogated in the absence and presence of a monolayer of carbon monoxide. The onset of activity for the hydrogen oxidation reaction is determined by reactivity mapping of these spatially localized compositions as a function of substrate electrode potential.

Experimental Section

Materials. *Reagents.* All experiments were performed using electrolytes in 18 MΩ deionized water (E-Pure, Barnstead, Dubuque, IA). Electrochemical measurements were performed in solutions containing as-received sulfuric acid (H_2SO_4) and sodium sulfate (Na_2SO_4) (Aldrich, Milwaukee, WI). Unless otherwise noted, the solutions were deaerated with nitrogen (BOC Gases, Murray Hill, NJ) prior to each measurement. Carbon monoxide coated surfaces were created by delivering pure CO gas (BOC Gases, Murray Hill, NJ) to the electrochemical apparatus by bubbling through a porous ceramic frit (Ace Glass, Inc., Vineland, NJ) into the electrolyte solution for a period of 5 min with the working electrode held under potential control. The CO was then removed from solution by purging with nitrogen for a period of 15 min. Deposits of Pt, Ru, and Mo were obtained by electrodeposition (vide infra) from solutions containing chloroplatinic acid (H_2PtCl_6), ruthenium chloride ($RuCl_3$), and sodium molybdate ($NaMoO_3$) (Strem Chemicals, Newburyport, MA) in 0.1 M Na_2SO_4. A Pt−Ir coated Ti mesh was used as counter electrode and a Hg/Hg_2SO_4 electrode was used as the reference electrode in all the electrochemical experiments. The potentials reported in this paper have been converted to the RHE scale.

Substrate Electrode Preparation. Indium−tin oxide (ITO) coated glass slides (Delta Technologies, Stillwater, MN) with a surface resistance of 100 Ω were used as substrates in this study and patterned to form an array of eight electrode bands. Each electrode was electrically isolated from others. The ITO substrates were cut into 25 mm × 37 mm sections using a diamond scribe followed by rinsing in copious amounts of deionized water, sonicating in a 50/50 ethanol/water mixture, rinsing again in deionized water, and finally drying thoroughly under a stream of nitrogen. A thin layer of the photoresist (Microposit S1813 Photoresist, Shipley, Marlborough, MA) was coated on the ITO substrate by spin coating at 1000 rpm. The substrate was soft-baked in a convection oven (Model 40 GC Lab Oven, Quincy Inc., Chicago, IL) at 100 °C for 30 min. This was followed by a 15-min exposure to ultraviolet light (UV source: Spectroline Model SB-100P, Spectronics Corp., Westbury, NY) through a patterned aluminum mask. The aluminum mask was prepared by the drilling of eight 1 mm wide bands with a separation of 1.5 mm through an aluminum plate of ∼0.7 mm thickness. This mechanical drilling was performed in our machine shop using a commercial drill press with an automated sample positioning system. The bandwidth and spacing were limited to feature sizes greater than approximately 0.5 mm due to the mechanical limitations of the drilling process. The substrate was developed immediately (Microposit MF-319 Developer, Shipley, Marlborough, MA), leaving behind the unexposed photoresist with the desired pattern. The substrate was subsequently rinsed in copious amounts of deionized water and hard-baked at 110 °C for 30 min. The ITO in the regions of the substrate that were not covered by the photoresist was etched from the surface by placing the sample in a solution containing 6 M HCl and 0.2 M HNO_3 for 15 min. The substrate was then rinsed thoroughly in deionized water and immersed in the photoresist remover (Microposit Remover 1165, Shipley, Marlborough, MA) for ∼2 min to remove the residual photoresist from the protected ITO regions. The substrate was then rinsed in deionized water, sonicated in a 50/50 ethanol/water mixture, rinsed again in deionized water, and dried thoroughly under a stream of nitrogen. A 12 mm × 24 mm × 30 mm rectangular glass tube with a wall thickness of 1.5 mm (Wale Apparatus Company, Inc., Hellertown, PA) was attached to the ITO substrate using Miccrostop stop-off lacquer (Pyramid Plastics Inc., Hope, AR) to form an electrochemical cell with a portion of each band electrode exposed outside the cell to provide electrical connection. The eight working electrodes were connected to a 20-pin dip clip (Pomona Electronics, Pomona, CA) to allow potential control of individual electrodes or the entire assembly.

Catalyst Samples. Pt_xRu_y and $Pt_xRu_yMo_z$ electrodes of varying composition were electrochemically deposited onto the ITO band electrodes. Solutions containing 10 mM H_2PtCl_6, 10mM $RuCl_3$, and 10 mM $NaMoO_3$ in 0.1M Na_2SO_4 were mixed in various ratios prior to deposition. The deposition procedure utilized a potential pulse program that applied a square wave to the band electrodes with potential limits of 0.5 and −1.0 V vs RHE at a frequency of 100 Hz with a potentiostat (Model 283, EG&G Instruments, Oakridge, TN) and a function generator (Global Specialities, New Haven, CT). Electrodeposition was carried out by injecting a solution of known metal composition into the electrochemical cell and applying the potential waveform to one of the eight electrode bands for a period of 5 min. Following deposition, the cell was thoroughly rinsed with deionized water before a new solution composition was injected. Electrodeposition was completed in a serial fashion until all electrodes were coated. For the Pt_xRu_y electrodes, the deposition solutions for the eight bands consisted of Pt/Ru solution with

molar ratios of 100/0, 90/10, 70/30, 40/60, 60/40, 30/70, 10/90, and 0/100. The $Pt_xRu_yMo_z$ electrodes were created using a mixture of the 90/10 Pt/Ru solution with varying Mo content. A set of four identical samples was prepared for each material and tested with a combination of scanning electrochemical microscopy (SECM), Auger electron spectroscopy (AES), scanning electron microscopy (SEM), energy-dispersive X-ray spectroscopy (EDS), and cyclic voltammetry.

Methods. *Scanning Electrochemical Microscope.* The scanning electrochemical microscope (SECM) used in this work was similar to that described in the literature,[66,67]and a complete description can be found elsewhere.[61,62] The electrochemical cell containing the band electrodes was positioned so that the plane of the substrate was oriented parallel to the SECM scanning plane with a multiaxis tilt stage (Model 39, Newport, Irvine, CA). Most experiments involved holding the tip potential at a value of −1.0 V vs RHE while changing the tip position and substrate potential. Line scans were acquired at several tip−sample separations at a tip scan rate of 200 μm s^{-1}. The SECM tips were fabricated with 25 μm diameter gold wires (Goodfellow, Berwyn, PA) sealed in glass using a technique similar to that described in the literature.[68] A more complete description can be found in our previous work.[61,62]

Multielectrode Potentiostat. Cyclic voltammetry was performed on the substrate electrodes using a multielectrode potentiostat (Model CH1030, CH Instruments Inc., Austin, TX), which could control eight working electrodes simultaneously. The working electrode leads were connected to eight of the pins of a 20-pin dip clip (Pomona Electronics, Pomona, CA), which was attached to the substrate electrode. A wound Pt−Ir counter electrode and a $Hg/HgSO_4$ reference electrode were used during voltammetry experiments. CO-stripping measurements were performed by dosing CO into the solution and adsorbing a monolayer on the electrode surfaces. CO was adsorbed on all eight electrodes simultaneously by holding the electrode potentials at a value of 0.05 V vs RHE for 5 min in a CO saturated solution with 0.01 M H_2SO_4/0.1 M Na_2SO_4. The CO was subsequently removed by purging with nitrogen for 5 min while still holding the potential at 0.05 V vs RHE. The potential of the electrodes were first scanned negative to 0 V vs RHE and then positive up to 0.9 V vs RHE at a scan rate of 0.1 V s^{-1}.

Scanning Electron Microscopy. Surface topography and bulk compositional analysis of the Pt_xRu_y and $Pt_xRu_yMo_z$ band electrodes was performed using a JEOL JXA 840A scanning electron microscope equipped with a X-ray detector (Princeton Gamma-Tech Inc., Princeton, NJ) for energy-dispersive spectroscopy (EDS) analysis. An accelerating voltage of 20 kV was used in all SEM experiments. A double-sided copper adhesive tape (3M Electrical Products Division, Austin, TX) was used to provide electrical contact between the substrate and the sample mount in order to prevent the charging effects during SEM measurements. The Pt Mα peak at 2.050 keV, the Ru Lα peak at 2.558 keV, and the Mo Lα peak at 2.293 keV were used to determine the bulk compositions of the band electrodes.

Auger Electron Spectroscopy. Surface compositions of the Pt_xRu_y band electrode were verified using a Model Φ560 Auger electron spectroscope (Physical Electronics, Eden Prairie, MN). An accelerating voltage of 3 kV was used in all AES measurements. Pt MNN peak at 69 eV and Ru MNN peak at 269 eV were used for the quantitative analysis of Pt and Ru. A double-sided copper adhesive tape was used to provide electrical contact between the substrate and the sample mount to prevent the charging effects.

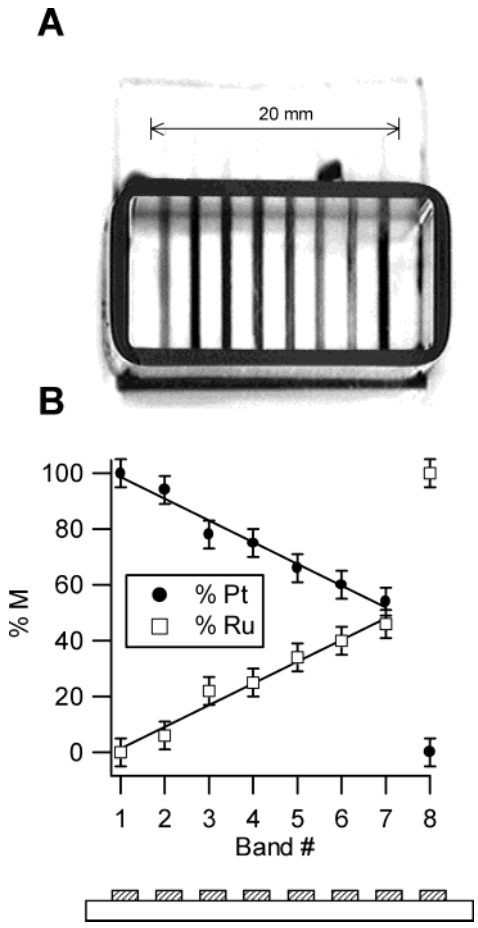

Figure 1. (A) Optical micrograph of eight-element band electrode. (B) Compositions of Pt_xRu_y band electrodse as determined by Auger electron spectroscopy (AES) with schematic of multielement band electrode (bottom).

Results and Discussion

Catalysts of various compositions were fabricated by electrochemical deposition onto multielement electrode band samples. The band electrodes consisted of eight individually addressable elements of 25 mm length, 1 mm width, and 1.5 mm separation created on an indium−tin oxide (ITO) coated, glass substrate via photolithography and etching. An image of the band electrode assembly is shown in Figure 1A. Electrodeposited catalysts were created by a pulsed potential program from solutions containing known compositions of the constituent metal salts. The Pt_xRu_y catalyst electrodes were deposited from solutions containing H_2PtCl_6 and $RuCl_3$ at various concentrations in 0.1 M Na_2SO_4. Following sample preparation, composition analysis was performed using a combination of Auger electron spectroscopy (AES) and energy-dispersive X-ray spectroscopy (EDS). Figure 1B (top) depicts the composition range of a typical Pt_xRu_y band sample as deduced by AES.

The Pt_xRu_y samples included eight electrodes with compositions ranging from pure Pt to pure Ru. AES was used to determine electrode compositions depicted in Figure 1. EDS compositional mapping provided essentially equivalent results for the various electrodes. The potential program used for deposition consisted of a symmetric square wave that varied between 0.50 and −1.0 V vs RHE at a frequency of 100 Hz. The application of a periodic potential waveform provided a more uniform particle size distribution than what could be achieved by constant potential deposition. This can be explained by considering that a brief negative potential favors particle

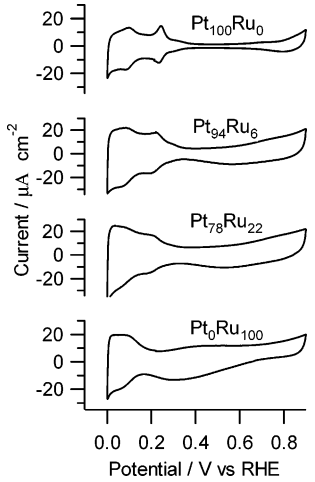

Figure 2. Cyclic voltammetry of selected Pt_xRu_y band electrodes in nitrogen-purged 0.01 M H_2SO_4/0.1 M Na_2SO_4 at a scan rate of 0.01 V s^{-1}.

nucleation while periodic excursions to positive potentials limit the time available for particle growth. Continued pulsing in this manner allows for an increase in particle number via nucleation, but maintains the particle size over a narrow range. In contrast, constant potential deposition tends to create a broad particle size distribution because particle nucleation and growth occurs continually throughout the deposition cycle.

Deposition was typically performed until a dense layer of particles formed with essentially uniform and complete coverage. SEM analysis of the deposits indicated that the morphology of the Pt_xRu_y catalysts consisted of spherical particles between 200 and 500 nm in diameter. A comparison of the composition of the deposition solution to the final deposition composition indicated that the catalyst samples prepared in this manner were slightly enriched in platinum compared to the bulk solution. For example, a deposition solution containing a molar Pt/Ru ratio of 90/10 gave a deposit with a composition ratio of 94/6 while a deposition solution with a Pt/Ru ratio of 10/90 gave a deposit with a composition near 50/50.

Cyclic voltammetry of the Pt_xRu_y samples in H_2SO_4 gives an indication of the composition of the samples and the influence of increasing Ru content (Figure 2). The pure platinum electrode (band 1, $Pt_{100}Ru_0$) behaves in a manner typical of polycrystalline platinum.[69] The two well-defined peaks and broad background current between 0.0 and 0.3 V reflect the underpotential deposition of hydrogen (H-UPD) that occurs on the various crystal planes exposed on a polycrystalline surface. Integration of the charge in the H-UPD region between 0.05 and 0.3 V can be used to estimate the active surface area, which for Figure 2 gives a value of 629 μC. Using a charge per unit area value of 210 μC cm^{-2} as the approximate number for polycrystalline platinum,[69] this gives an electrode area of approximately 3 cm^2, which corresponds to a roughness factor of about 20. Since the H-UPD region for Ru-containing samples also includes contributions from hydrogen absorption, this calculation does not provide an accurate measure of the surface area of Pt_xRu_y samples.[70] A comparison of the SEM photos of the various Pt_xRu_y electrodes indicates a similar particle size and coverage, so the Pt surface area was used as an estimate of the surface areas for the other electrodes.

Increasing the potential of the $Pt_{100}Ru_0$ electrode produces features corresponding to the double layer and then oxide formation. The current in the double layer region between 0.3 and 0.7 V is featureless and reflects a clean metal surface. Platinum hydroxide and oxide formation commence at potentials approaching 0.8 V. Reversing the potential scan direction at 0.85 V results in cathodic current corresponding to the reduction of platinum oxides. Further negative excursions in the electrode potential produce signatures of the double layer (0.7−0.3 V) and H-UPD (0.3−0 V) regions as near-mirror images of the positive-going scan.

The pure ruthenium electrode (band 8, Pt_0Ru_{100}) differs from pure platinum in a number of respects. The H-UPD region between 0.0 and 0.2 V displays a broad response without well-defined peaks. Current measured in this region includes contributions from both hydrogen adsorption onto the ruthenium surface and significant hydrogen absorption into the bulk of the metal.[70] At potentials below 0.3 V, ruthenium exists in the metallic state.[71] Positive excursions in the electrode potential above 0.3 V create ruthenium hydroxides and oxides. Ruthenium oxides exhibit a large capacitance as evidenced by the increased charging current in the double layer region between 0.3 and 0.7 V. The oxide content of ruthenium has been shown to be potential dependent with complete conversion of surface ruthenium to oxides occurring by 0.95 V vs RHE.[72,73] Further positive excursions in the electrode potential above 0.95 V lead to dissolution of the Ru oxides and irreversible loss of Ru from the electrode surface. Reduction of the Ru oxides back to Ru metal appears as a broad reduction peak located between 0.5 and 0.2 V on the negative potential scan.

Figure 2 also depicts two of the intermediate composition Pt_xRu_y electrodes at $Pt_{94}Ru_6$ and $Pt_{78}Ru_{22}$. Both compositions exhibit a character that combines features of pure Pt and pure Ru. The H-UPD region on $Pt_{94}Ru_6$ displays a broadened overall response with suppressed strong and weak adsorption peaks compared to pure Pt. The charging current in the double layer region is increased in magnitude. The $Pt_{78}Ru_{22}$ electrode exhibits further suppression of the strong and weak adsorption peaks and increased capacitive current in the double layer region. Both intermediate composition electrodes exhibit a broad reduction peak near 0.5 V that is presumably due to the reduction of Ru oxides.

Scanning electrochemical microscope (SECM) measurements were performed to examine the activity of the various Pt_xRu_y electrodes toward the hydrogen oxidation reaction. This was achieved by using the proton/hydrogen redox couple as the SECM tip reaction.[63−65] In these experiments, the tip electrode was held at a constant potential of −1.0 V vs RHE. At this potential, the tip reaction is the diffusion-limited reduction of protons to hydrogen:

$$2H^+ + 2e^- \rightarrow H_2 \qquad (1)$$

The steady-state tip current for this reaction achieves a value of approximately −340 nA for a 25 μm diameter electrode in a solution containing 10 mM H_2SO_4. Far from a substrate surface, the tip current remains constant at this value. Positioning the tip near a substrate surface causes the tip current to change from the diffusion-limited value. At a nonreactive substrate such as glass, the tip current decreases in magnitude as the substrate is approached due to hindered diffusion of protons from bulk solution to the tip. If the tip is positioned near a surface that acts as a catalyst for hydrogen oxidation, the tip current increases. This occurs because the substrate can oxidize the hydrogen that is produced at the tip back to protons according to

$$H_2 \rightarrow 2H^+ + 2e^- \qquad (2)$$

SCHEME 1: Schematic of Tip−Substrate Interface during Scanning Electrochemical Microscopy of the Hydrogen Oxidation Reaction: (A) Active Substrate; (B) CO-Covered Substrate

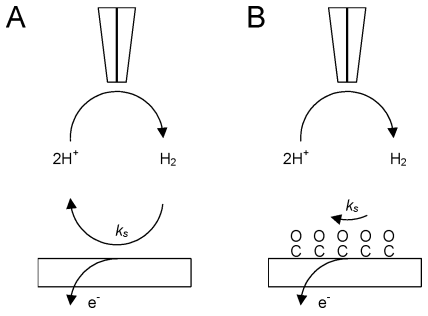

The protons that are produced at the substrate diffuse back to the tip and are reduced back to hydrogen (Scheme 1A). This results in an increase in the tip current (termed positive feedback) that is a function of both the tip−sample separation and the substrate rate constant (k_s) for hydrogen oxidation.[74] Since the SECM samples only a small volume of solution in close proximity to the tip electrode, the current response can provide information concerning the local reactivity of a substrate. In this work, the tip electrode was used to map the local reactivity of the multielement band electrodes toward the hydrogen oxidation reaction. Scanning the tip electrode over the electrode bands containing various catalyst compositions while simultaneously measuring the tip current was used to deduce catalyst activity.

Figure 3A depicts a series of line scans measured with the SECM tip scanned over an eight-element Pt_xRu_y band sample. The band numbers corresponding to the compositions depicted in Figure 1 are listed. Each line in the figure represents a scan taken at a fixed tip−sample separation with the tip electrode scanned for a lateral distance of 20 mm at a velocity of 200 μm s^{-1} from left of the first to right of the eighth band. At a separation of 60 μm, seven of the bands appear as small features with a slightly increased tip current on top of a uniform background value. Scans taken at separations greater than 100 μm were essentially featureless. Decreasing the tip−sample separation from 60 μm down to 10 μm increases the magnitude of the tip current over bands 1−7. The tip current over the insulating regions between the electrode bands and over band 8 (pure Ru) decreases as the tip−sample separation is reduced. The increase in tip current over bands 1−7 and the decrease in current over band 8 and the insulating regions can be explained in terms of the magnitude of the rate constant (k_s) for the hydrogen oxidation reaction at these substrate locations.

Figure 3B depicts the tip current over each of the band electrodes plotted as a function of tip−sample separation. Each of the bands 1−7 exhibits an identical response that shows an increase in tip current as the tip−sample separation is reduced. These bands represent Pt_xRu_y compositions between pure Pt and $Pt_{54}Ru_{46}$. The increase in tip current can be interpreted as a pure positive feedback response that reflects a rate constant for hydrogen oxidation over these regions of the substrate that is in excess of 1 cm s^{-1}, which is the maximum rate constant detectable by the tip in the current configuration.[64] The eighth band, which is pure Ru, displays a decrease in current with tip−sample approach that is consistent with pure negative feedback and reflects an inactive surface with a rate constant for hydrogen oxidation below 0.001 cm s^{-1}. These results demonstrate that the Pt_xRu_y electrodes with a Ru content below 50% prepared by this pulsed electrodeposition procedure exhibit high activity for the hydrogen oxidation reaction. This activity can be described by a rate constant in excess of 1 cm s^{-1} for all but the pure Ru band.

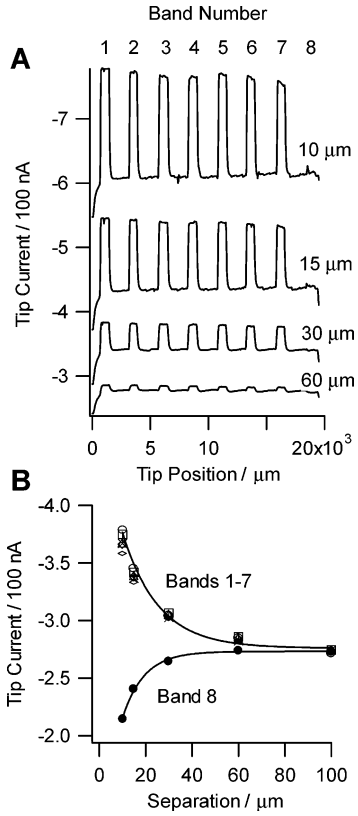

Figure 3. (A) SECM line scans over Pt_xRu_y band electrodes as a function of tip−substrate separation in nitrogen-purged 0.01 M H_2SO_4/0.1 M Na_2SO_4. The tip potential is held at −1.0 V vs RHE, while the substrate potential is held at 0.1 V vs RHE. Each curve is offset vertically for clarity. (B) Tip current as a function of tip−substrate separation directly above the band electrodes. The solid lines are drawn as a guide to the eye and represent positive (upper) and (lower) negative feedback responses.

Carbon monoxide is known to strongly adsorb to platinum and deactivate that surface toward hydrogen oxidation by blocking sites for hydrogen adsorption.[4,5] Since CO is present in hydrogen fuels produced by the reforming of hydrocarbons, it is important to understand the influence of this species on hydrogen oxidation. It is also important to identify catalysts that can effectively mitigate the impact of CO poisoning at low potentials either by promoting its oxidation or by reducing the surface coverage to a level where sufficient hydrogen oxidation rates can be achieved.

In typical electrochemical measurements studying the influence of CO on hydrogen oxidation, both components are fed to a rotating disk electrode.[5,8] An alternative to this approach is to use the SECM to measure the kinetics of hydrogen oxidation in the presence of carbon monoxide.[64,65] With this technique, CO is delivered to the electrode surface from solution while hydrogen is generated locally at the SECM's microelectrode tip. For a gold microelectrode reducing protons to hydrogen, the tip response is unaffected by the presence of CO in solution. Therefore, the tip current reflects only the diffusion-limited proton reduction rate and changes in that value due to feedback from a substrate. Thus, the SECM effectively decouples the measured signal from the CO oxidation current. This allows the SECM to probe hydrogen oxidation in the presence of a CO layer without it influencing the accuracy or interpretation of the tip response. In this work, we use this facility to probe

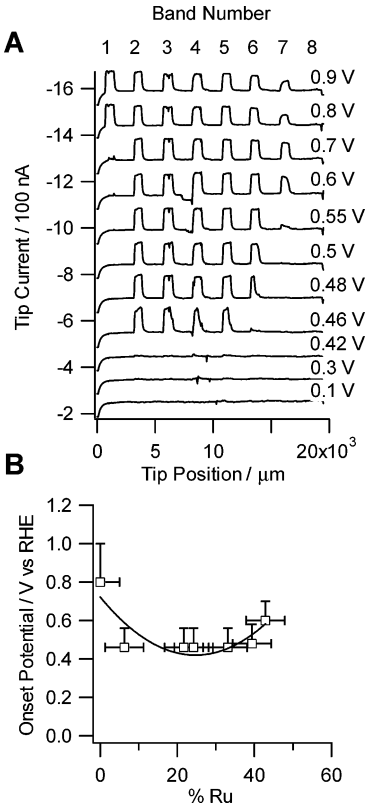

Figure 4. (A) SECM line scans over CO-coated Pt_xRu_y band electrodes at a tip−substrate separation of 15 μm in nitrogen-purged 0.01 M H_2SO_4/0.1 M Na_2SO_4 with the tip potential held at −1.0 V. Each curve is offset vertically for clarity. (B) Summary of onset potentials for hydrogen oxidation on CO-coated Pt_xRu_y electrodes. The solid line has been added to serve as a guide to the eye.

the activity and the onset potential of various catalysts toward the hydrogen oxidation reaction on a CO-poisoned surface.

Figure 4A depicts a series of SECM line scans over the Pt_xRu_y band electrodes taken at a tip−sample separation of 15 μm. These results illustrate the impact of an adsorbed CO layer on the hydrogen oxidation reaction for these electrode compositions. The band numbers corresponding to the compositions listed in Figure 1 are depicted at the top of Figure 4A. The line scans were acquired following exposure of the substrate electrodes to CO gas for a period of 5 min while the electrodes were held at a potential of 0.05 V. Following adsorption of a monolayer of CO, the solution was purged with nitrogen. The bottom curve in Figure 4a was acquired with the substrate potential at 0.1 V and indicates complete inactivity at all electrode bands (Scheme 1B). The curve depicts a constant negative feedback in which the band electrodes are indistinguishable from the insulating regions between them and the surface appears uniform. Thus, the hydrogen oxidation reaction is completely suppressed by adsorbed CO at all catalyst compositions at this electrode potential.

Additional SECM line scans were acquired at increasingly positive substrate potentials. At 0.3 and 0.42 V, all electrodes remain inactive. However, at 0.46 V electrodes 2−5 exhibit an increased tip current. This increase in current reflects positive feedback between tip and sample due to the onset of hydrogen oxidation at the substrate. Presumably, this activation occurs in concert with carbon monoxide oxidation from the surface that frees active surface sites for hydrogen adsorption and subsequent oxidation. Notably, this activation does not reflect complete oxidation of the CO monolayer, but rather indicates the early stages of this process. Hydrogen oxidation can occur after the removal of only a fraction of the CO layer (vide infra).[5,65]

The compositions of the most active electrodes 2−5 vary in ruthenium content from 6 to 34%. As the substrate potential is further increased, additional electrodes start to activate. Between 0.48 and 0.5 V, electrode 6 with a ruthenium composition of 40% becomes active and electrode 7, with a ruthenium composition of 46%, activates between 0.55 and 0.6 V. The pure platinum electrode becomes active at 0.8 V, while the pure ruthenium electrode remains inactive over the entire potential range.

A summary of the onset potential values as determined by SECM imaging of the Pt_xRu_y electrodes is depicted in Figure 4B. The criteria set for the onset potential is the value where the tip current is at least 50% of its value in the absence of adsorbed CO on the catalyst at a given tip−substrate separation. This series of binary catalysts exhibits a broad minimum in the onset potential for hydrogen oxidation at roughly 0.45 V for electrodes with Ru contents between 5 and 40%. These onset potentials are nearly 0.35 V lower than that exhibited by pure platinum.

Hydrogen oxidation on these CO-poisoned electrodes is suppressed at low potentials due to the decrease in available surface sites for the adsorption and dissociation of hydrogen. In order for the hydrogen oxidation reaction to proceed, CO must be removed via oxidation to CO_2. The bifunctional mechanism can be used to describe the mechanism of CO removal.[75−77] CO is oxidized from platinum sites (Pt) following the dissociation of water on neighboring metal sites (M):

$$M + H_2O \rightarrow M{-}OH + H^+ + e^- \quad (3)$$

Water dissociation forms metal hydroxides (or oxides), which can convert CO to CO_2 according to

$$Pt{-}CO + M{-}OH \rightarrow Pt + M + CO_2 + H^+ + e^- \quad (4)$$

Since the rate of the hydrogen oxidation on platinum is large, it is possible to reach mass transport limited oxidation rates with only a small number of CO-free surface sites.[5] Therefore, hydrogen oxidation activates following the removal of only a fraction of the CO monolayer. In fact, it has been shown that a decrease in as little as 10% of a monolayer is sufficient to increase the rate of hydrogen oxidation from near zero to diffusion-limited values.[65] This is in contrast to methanol oxidation, where a greater number of surface sites are required to adsorb and dissociate methanol.[78−80]

On pure platinum, CO oxidation occurs in concert with oxide formation and typically is observed in the neighborhood of 0.8 V for polycrystalline electrodes.[69] This behavior is consistent with the onset potential for hydrogen oxidation measured for the pure platinum electrode (Figure 4B). Ruthenium, in contrast, dissociates water to form oxides at a considerably lower potential than platinum as is illustrated in the base electrode voltammetry in Figure 2. Ruthenium oxidation and the dissociation of water commence between 0.4 and 0.6 V on pure ruthenium. The ability of the Pt_xRu_y electrodes to oxidize hydrogen in the presence of adsorbed CO is a combination of the presence of Ru sites to dissociate water and subsequently oxidize CO and Pt sites to adsorb and dissociate hydrogen. The broad "optimum" Ru composition range observed between 5 and 40% reflects the presence of sufficient Ru to initiate CO oxidation and free enough Pt sites to achieve mass transport limited oxidation rates for hydrogen which is in agreement with the RDE studies carried

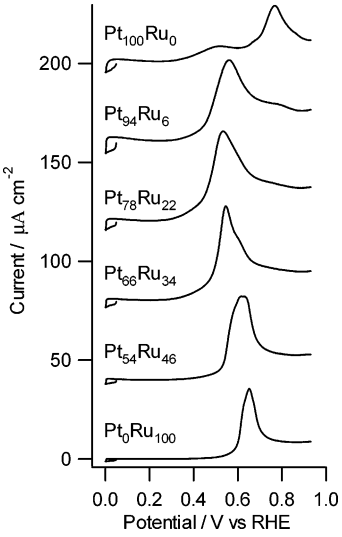

Figure 5. Cyclic voltammetry of CO-coated Pt_xRu_y band electrodes in nitrogen-purged 0.01 M H_2SO_4/0.1 M Na_2SO_4 at a scan rate of 0.01 V s^{-1}.

out on Pt_xRu_y bulk electrodes.[8,9] In the experiments performed here, the diffusion-limited oxidation rate reflects a rate constant in excess of 1 cm s^{-1}. Notably, a surface containing as little as 5% Ru can oxidize a sufficient quantity of CO from the Pt sites to produce mass transport limited hydrogen oxidation.

CO stripping voltammetry on a selection of the Pt_xRu_y electrodes is depicted in Figure 5. In these experiments, a monolayer of CO was adsorbed onto the various electrodes for a period of 5 min with the electrodes held at 0.05 V. The solution was subsequently purged with nitrogen and the electrode potentials were then scanned in the positive direction so as to oxidize the CO layer. These results display the typical response of Pt_xRu_y electrodes during CO oxidation.[81] The pure Pt electrode exhibits two oxidation peaks on the positive scan. A broad, shallow oxidation peak appears between 0.4 and 0.7 V. This peak is often referred to as a "prewave" and reflects oxidation of weakly adsorbed CO ($CO_{ads,w}$).[5] On Pt(111) surfaces, this oxidation is a transient phenomenon corresponding to a phase transition of the CO monolayer from an ordered C(2 $\times$ 2) structure with a coverage of 0.75 monolayer to a disordered structure with a coverage of 0.68 monolayer.[82,83] Both surfaces completely poison the platinum surface toward hydrogen oxidation under steady-state conditions.[5] The main oxidation peak at 0.8 V corresponds to complete removal of the CO layer by oxidation of strongly adsorbed CO ($CO_{ads,s}$).

The oxidation of CO on the various Pt_xRu_y electrodes proceeds without a noticeable prewave but with an onset potential and peak potential that appear at lower potentials than Pt and are composition dependent. The pure Ru electrode exhibits a CO oxidation peak at 0.65 V. Increasing the platinum content produces a lower peak potential for CO oxidation, with a minimum exhibited at approximately 0.5 V for the electrodes with Ru contents between 5 and 35%. This trend is consistent with prior results for electrodeposited Pt_xRu_y electrodes,[81,84,85] although work using electrode preparations that include bulk alloys[86,87] and chemically synthesized nanoparticles[88,89] report minimum peak potential values for Ru compositions that vary between 10 and 50%. As mentioned earlier, hydrogen oxidation can occur on CO-covered surfaces once active sites begin to form due to the onset of CO oxidation. Thus, the peak potential is less important for this process than the onset potential for CO oxidation. In Figure 5, it is clear that the onset of CO oxidation occurs at considerably lower potentials than the peak

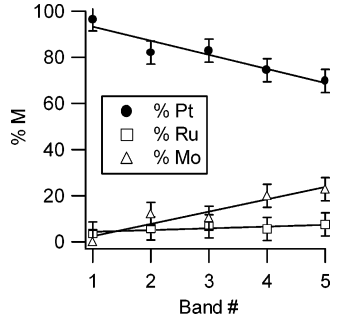

Figure 6. Composition of $Pt_xRu_yMo_z$ electrodeposited catalyst bands as determined by energy-dispersive X-ray spectroscopy (EDS).

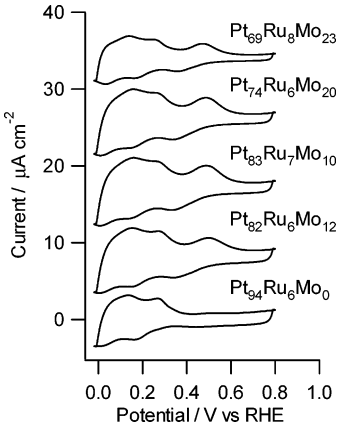

Figure 7. Cyclic voltammetry of $Pt_xRu_yMo_z$ band electrodes in nitrogen-purged 0.01 M H_2SO_4/0.1 M Na_2SO_4 at a scan rate of 0.01 V s^{-1}.

potential. In particular, the electrodes with Ru compositions of 6, 22, and 34% exhibit an onset for CO oxidation at a potential near 0.4 V. The onset potentials for CO oxidation in Figure 5 are consistent with the values measured for hydrogen oxidation on these surfaces in Figure 4B.

A variety of multicomponent catalysts have been constructed in an attempt to improve performance for the oxidation of fuels such as H_2/CO and methanol. Additional components have been added to improve poison tolerance, promote water dissociation at lower potentials, and activate C−C and C−O bond breaking. The hydrogen oxidation reaction requires platinum sites to adsorb and dissociate hydrogen while CO tolerance is obtained by introducing metals that promote the dissociation of water at low potentials. Binary systems with platinum and either tin or molybdenum have shown favorable performance compared to ruthenium.[14,15] In an attempt to explore the impact of molybdenum content on the hydrogen oxidation reaction in the presence of adsorbed CO, we have constructed and characterized a series of $Pt_xRu_yMo_z$ electrodes.

Figure 6A depicts the compositions of five electrode bands constructed by pulsed potential electrodeposition from solutions containing varying amounts of H_2PtCl_6, $RuCl_3$, and $NaMoO_3$. The deposition procedure was the same as that used to create the Pt_xRu_y electrodes (vide supra). The solution concentrations were selected to reside in the platinum-rich region of the ternary phase diagram of Pt−Ru−Mo with a Ru content between 5 and 8%. The five electrodes depicted in Figure 6 possess a Mo content within the range of a minimum of 0% to a maximum of 23%.

Cyclic voltammetry of the $Pt_xRu_yMo_z$ electrodes depicts a behavior that differs from pure Pt, pure Ru, and the Pt_xRu_y electrodes (Figure 7). The Mo-free electrode, denoted $Pt_{94}Ru_6Mo_0$, exhibits the characteristic signature for Pt_xRu_y that includes

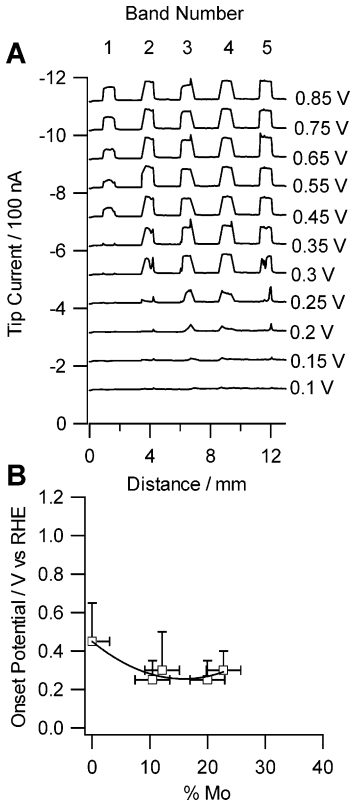

Figure 8. (A) SECM line scans over CO-coated $Pt_xRu_yMo_z$ band electrodes at a tip−substrate separation of 10 μm in nitrogen-purged 0.005 M H_2SO_4/0.1 M Na_2SO_4 with the tip potential held at −1.0 V. Each curve is offset vertically for clarity. (B) Summary of onset potential for hydrogen oxidation on CO-coated $Pt_xRu_yMo_z$ electrodes. The solid line has been added to serve as a guide to the eye.

a combination of Pt and Ru behavior. The addition of Mo to this nominal electrode composition produces additional electrochemical current in the potential range between 0.3 and 0.6 V. A distinct oxidation peak is observed in all Mo-containing electrodes at a potential of about 0.5 V with a corresponding reduction peak at 0.35 V. The remainder of the voltammogram resembles that of the $Pt_{94}Ru_6Mo_0$ electrode with a similar capacitive current at the positive potential limit and hydrogen adsorption peaks of a similar magnitude and shape.

The additional current in the potential range from 0.3 to 0.6 V for the Mo-containing electrodes suggests that the Mo component is undergoing an oxidation/reduction process. The Pourbaix diagram for Mo suggests a stable oxide of composition MoO_2 or MoO_3 will form in this potential/pH range.[90] Therefore, it is reasonable to speculate that these Mo-containing electrodes will be able to dissociate water and provide hydroxide or oxide surface species that are able to oxidize carbon monoxide at low potentials.

Characterization of this series of $Pt_xRu_yMo_z$ electrodes using SECM reactivity mapping supports the idea of enhanced activity. Line scans over the various Mo-containing electrodes in the absence of CO (*not shown*) indicate that all compositions exhibit diffusion-limited oxidation rates for hydrogen oxidation. This is reasonable in that the Pt content in these electrodes remains above 75%, which provides sufficient active sites for hydrogen oxidation to achieve diffusion-limited oxidation rates.

Figure 8A illustrates a series of SECM line scans acquired at a tip−sample separation of 10 μm following adsorption of a monolayer of CO from solution. The substrate electrode was held at 0.05 V for 5 min in a CO-saturated solution before purging with nitrogen. The line scan acquired at 0.1 V exhibits

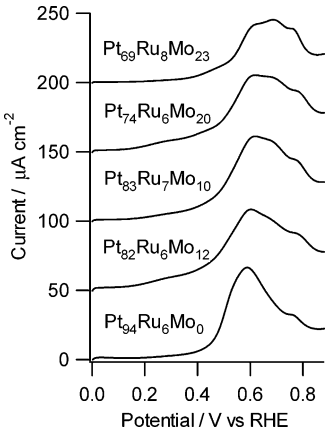

Figure 9. Cyclic voltammetry of CO-coated $Pt_xRu_yMo_z$ band electrodes in nitrogen-purged 0.01 M H_2SO_4/0.1 M Na_2SO_4 at a scan rate of 0.01 V s^{-1}.

pure negative feedback over the entire electrode surface, which indicates that the $Pt_xRu_yMo_z$ electrodes are completely inactive toward hydrogen oxidation due to poisoning by CO. All electrodes remain inactive as the substrate potential is increased to 0.2 V. At 0.20 V, however, the electrodes with compositions $Pt_{83}Ru_7Mo_{10}$ and $Pt_{74}Ru_6Mo_{20}$ start to exhibit positive feedback, which indicates that the surfaces have a reduced CO coverage and are starting to oxidize hydrogen. At 0.3 V, all four of the Mo-containing electrodes are actively oxidizing hydrogen. This is presumably the result of removal of a portion of the CO monolayer and the creation of free Pt sites. Consistent with the previous results from Figure 4, the $Pt_{94}Ru_6Mo_0$ electrode activates near 0.45 V.

A summary of the onset potential values for the Mo-containing electrodes is given in Figure 8B. As clearly noted, the addition of Mo decreases the onset potential for hydrogen oxidation by nearly 0.2 V compared to the best Pt_xRu_y electrodes. The Mo compositions between 10 and 25% appear equally active within experimental error. The improved performance of these electrodes is likely due to the ability of the Mo component to promote CO oxidation at lower potentials. Notably, a recent study examining Mo adlayers on single crystal platinum surfaces using differential electrochemical mass spectrometry postulates that Mo is converting a fraction of the CO on Pt to a weakly adsorbed state due to an oxygen spillover effect.[91]

Cyclic voltammetry of the $Pt_xRu_yMo_z$ electrodes following the adsorption of the CO monolayer is consistent with the behavior observed by SECM mapping. Figure 9 illustrates the stripping voltammetry for a CO monolayer adsorbed on these electrodes. The $Pt_{94}Ru_6Mo_0$ electrode exhibits a sharp oxidation wave with an onset that commences near 0.4 V and a peak at 0.6 V. In contrast, the Mo-containing electrodes exhibit a broadening of the oxidation wave and an earlier onset potential. The onset of anodic current, which corresponds to the start of CO oxidation, occurs at a potential near 0.2 V, while the peak of the oxidation wave occurs at a potential very near that of the Mo-free electrode. The onset potential values for CO oxidation are consistent with the onset of hydrogen oxidation as determined by SECM scanning.

The results of this study are summarized on the ternary composition diagram shown in Figure 10. The various compositions studied are identified with circles on the Pt−Ru−Mo diagram. The size of the circles reflects the onset potentials measured for hydrogen oxidation with the SECM. The larger spots reflect lower onset potentials. The ability of both Ru and

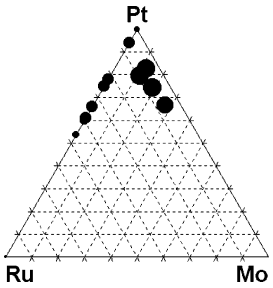

Figure 10. Ternary phase diagram showing compositions examined in this study. The marker size reflects the onset potential for hydrogen oxidation with the largest markers representing the lowest onset potential.

Mo to dissociate water at low potentials to provide surface hydroxides or oxides promotes CO oxidation. Notably, hydrogen oxidation proceeds in these systems at very high rates so that very few surface Pt sites are necessary to allow diffusion-limited oxidation rates. Thus, the onset potentials measured with SECM correspond to the very early stages of CO oxidation and do not require complete monolayer removal. The present results are also consistent with those of several studies involving infrared spectroscopy to determine the onset potentials for CO oxidation on various Pt_xRu_y electrodes.[16,87,92] In addition to determining the onset potential for CO oxidation, SECM also allows one to determine the reaction rates for hydrogen oxidation at these potentials, indicating the potential at which practical current densities can be achieved for hydrogen oxidation in the presence of CO.

Further improvements in catalyst performance for hydrogen oxidation in the presence of dissolved or surface CO may be achieved by creating electrodes with Pt and metals that dissociate water at lower potentials. Notably, these materials are restricted by the ability to form stable oxides that do not actively dissolve in a low-pH environment. Notably, both Mo and Sn, which dissociate water at lower potentials than Ru, exhibit Pourbaix diagrams that suggest the formation of soluble oxides over a range of potentials in acidic pH conditions, which may limit their utility in commercial fuel cell electrodes. However, components such as W, Ta, Nb, or Ti are promising candidates for further study due to the formation of stable oxides at low potentials in acidic environments.

Conclusions

This paper demonstrated an application of the scanning electrochemical microscope (SECM) as a screening tool for combinatorial studies of fuel cell catalysts. This technique is particularly useful for indirectly measuring the onset of hydrogen oxidation through a catalyst surface that has been poisoned with a strongly bound adsorbate such as carbon monoxide. With the use of SECM, the hydrogen oxidation activity and poison (CO) tolerance of the catalysts are effectively decoupled. The onset of CO oxidation as well as the rate of hydrogen oxidation at these potentials could be quantitatively determined using this approach. The ability of Pt_xRu_y electrodes to oxidize hydrogen in the presence of a CO monolayer at potentials 0.35 V below that of pure Pt demonstrates the ability of Ru to dissociate water at potentials much lower than Pt. Mo-containing electrodes improved the onset potential by an additional 0.2 V. We are currently extending this methodology to examine additional regions of composition space in the $Pt_xRu_yMo_z$ system as well as multicomponent electrodes with additional metals that exhibit stable oxide formation at low potentials.

Acknowledgment. The authors thank the Office of Naval Research for a Young Investigator Award, the National Science Foundation for a CAREER Award, the Camille and Henry Dreyfus Foundation for a New Faculty Award, and the donors of the Petroleum Research Fund as administered by the American Chemical Society for partial support of this research. We also thank Catherine Dukes of the University of Virginia Surface Science Laboratory for assisting with AES measurements.

References and Notes

(1) Appleby, A. J.; Foulkes, F. R. *Fuel Cell Handbook*; Van Nostrand Reinhold: New York, 1989.
(2) Larminie, J.; Dicks, A. *Fuel Cell Systems Explained*, 1st ed.; Wiley: New York, 2000.
(3) Ross, P. N. In *Electrocatalysts*; Ross, P. N., Lipkowski, J., Eds.; Wiley: New York, 1998; pp 1−75.
(4) Kita, H.; Naohara, H.; Nakato, T.; Taguchi, S.; Aramata, A. *J. Electroanal. Chem.* **1995**, *386*, 197−206.
(5) Markovic, N. M.; Grgur, B. N.; Lucas, C. A.; Ross, P. N. *J. Phys. Chem. B* **1999**, *103*, 487−495.
(6) Watanabe, M.; Motoo, S. *Electroanal. Chem. Interfac. Electrochem.* **1975**, *60*, 267−273.
(7) Watanabe, M.; Uchida, M.; Motoo, S. *J. Electroanal. Chem.* **1987**, *229*, 395−406.
(8) Gasteiger, H. A.; Markovic, N. M.; Ross, P. N. *J. Phys. Chem.* **1995**, *99*, 8290−8301.
(9) Gasteiger, H. A.; Markovic, N. M.; Ross, P. N. *J. Phys. Chem.* **1995**, *99*, 16757−16767.
(10) Chrzanowski, W.; Kim, H.; Wieckowski, A. *Catal. Lett.* **1998**, *50*, 69−75.
(11) Rolison, D. R.; Hagans, P. L.; Swider, K. E.; Long, J. W. *Langmuir* **1999**, *15*, 774−779.
(12) Grgur, B. N.; Zhuang, G.; Markovic, N. M.; Ross, P. N. *J. Phys. Chem. B* **1997**, *101*, 3910−3913.
(13) Nakajima, H.; Kita, H. *Electrochim. Acta* **1990**, *35*, 849−853.
(14) Grgur, B. N.; Markovic, N. M.; Ross, P. N. *J. Electrochem. Soc.* **1999**, *146*, 1613−1619.
(15) Gasteiger, H. A.; Markovic, N. M.; Ross, P. N. *J. Phys. Chem.* **1995**, *99*, 8945−8949.
(16) Morimoto, Y.; Yeager, E. B. *J. Electroanal. Chem.* **1998**, *441*, 77−81.
(17) Paffett, M. T.; Gebhard, S. C.; Windham, R. G.; Koel, B. E. *J. Phys. Chem.* **1990**, *94*, 6831−6839.
(18) Zhu, Y. M.; Cabrera, C. R. *Electrochem. Solid State Lett.* **2001**, *4*, A45−A48.
(19) Ley, K. L.; Liu, R. X.; Pu, C.; Fan, Q. B.; Leyarovska, N.; Segre, C.; Smotkin, E. S. *J. Electrochem. Soc.* **1997**, *144*, 1543−1548.
(20) Motoo, S.; Okada, T. *J. Electroanal. Chem.* **1983**, *157*, 139−144.
(21) Grgur, B. N.; Markovic, N. M.; Ross, P. N. *Electrochim. Acta* **1998**, *43*, 3631−3635.
(22) Schmidt, T. J.; Stamenkovic, V.; Attard, G. A.; Markovic, N. M.; Ross, P. N. *Langmuir* **2001**, *17*, 7613−7619.
(23) Oetjen, H.-F.; Schmidt, V. M.; Stimming, U.; Trila, F. *J. Electrochem. Soc.* **1996**, *143*, 3838−3842.
(24) Gurau, B.; Viswanathan, R.; Liu, R. X.; Lafrenz, T. J.; Ley, K. L.; Smotkin, E. S.; Reddington, E.; Sapienza, A.; Chan, B. C.; Mallouk, T. E.; Sarangapani, S. *J. Phys. Chem. B* **1998**, *102*, 9997−10003.
(25) Maier, W. F. *Angew. Chem., Int. Ed.* **1999**, *38*, 1216−1218.
(26) Jandeleit, B.; Schaefer, D. J.; Powers, T. S.; Turner, H. W.; Weinberg, W. H. *Angew. Chem., Int. Ed.* **1999**, *38*, 2495−2532.
(27) Andrus, M. B.; Turner, T. M.; Sauna, Z. E.; Ambudkar, S. V. *J. Org. Chem.* **2000**, *65*, 4973−4983.
(28) Jandeleit, B.; Weinberg, H. *Chem. Ind.* **1998**, *19*, 795−798.
(29) Pescarmona, P. P.; van der Waal, J. C.; Maxwell, I. E.; Maschmeyer, T. *Catal. Lett.* **1999**, *63*, 1−11.
(30) Wang, J.; Yoo, Y.; Gao, C.; Takeuchi, I.; Sun, X.; Chang, H.; Xiang, X.-D.; Schultz, P. G. *Science* **1998**, *279*, 1712−1714.
(31) Danielson, E.; Golden, J. H.; McFarland, E. W.; Reaves, C. M.; Weinberg, W. H.; Wu, X. D. *Nature* **1997**, *389*, 944−948.
(32) Schlogl, R. *Angew. Chem., Int. Ed.* **1998**, *37*, 2333−2336.
(33) Brouwer, A. J.; van der Linden, H. J.; Liskamp, R. M. J. *J. Org. Chem.* **2000**, *65*, 1750−1757.
(34) Maxwell, I. E. *Nature* **1998**, *394*, 325−326.
(35) Hill, C. L.; Gall, R. D. *J. Mol. Catal. A* **1996**, *114*, 103−111.
(36) Snively, C. M.; Oskarsdottir, G.; Lauterbach, J. *Catal. Today* **2001**, *67*, 357−368.
(37) Yoshida, H.; Murata, C.; Hattori, T. *J. Catal.* **2000**, *194*, 364−372.

(38) Huo, Q.; Sui, G.; Kele, P.; Leblanc, R. M. *Angew. Chem., Int. Ed.* **2000**, *39*, 1854−1857.
(39) Jaramillo, T. F.; Ivanovskaya, A.; McFarland, E. W. *J. Comb. Chem.* **2002**, *4*, 17−22.
(40) Suchanek, W. L.; Watanabe, T.; Sakurai, B.; Kumagai, N.; Yoshimura, M. *Rev. Sci. Instrum.* **1999**, *70*, 2432−2437.
(41) Klein, J.; Lehmann, C. W.; Schmidt, H.-W.; Maier, W. F. *Angew. Chem., Int. Ed.* **1998**, *37*, 3369−3372.
(42) van Dover, R. B.; Schneemeyer, L. F.; Flaming, R. M.; Huggins, H. A. *Biotechnol. Bioeng.* **1999**, *61*, 217−225.
(43) Reddington, E.; Sapienza, A.; Gurau, B.; Viswanathan, R.; Sarangapani, S.; Smotkin, E. S.; Mallouk, T. E. *Science* **1998**, *280*, 1735−1737.
(44) Cong, P. J.; Doolen, R. D.; Fan, Q.; Giaquinta, D. M.; Guan, S. H.; McFarland, E. W.; Poojary, D. M.; Self, K.; Turner, H. W.; Weinberg, W. H. *Angew. Chem., Int. Ed.* **1999**, *38*, 484−488.
(45) Hoffmann, C.; Wolf, A.; Schuth, F. *Angew. Chem., Int. Ed.* **1999**, *38*, 2800−2803.
(46) Holzwarth, A.; Schmidt, H.-W.; Maier, W. F. *Angew. Chem., Int. Ed.* **1998**, *37*, 2664−2647.
(47) Cong, P. J.; Dehestani, A.; Doolen, R.; Giaquinta, D. M.; Guan, S. H.; Markov, V.; Poojary, D.; Self, K.; Turner, H.; Weinberg, W. H. *Proc. Natl. Acad. Sci. U.S.A.* **1999**, *96*, 11077−11080.
(48) Sullivan, M. G.; Utomo, H.; Fagan, P. J.; Ward, M. D. *Anal. Chem.* **1999**, *71*, 4369−4375.
(49) Taylor, S. J.; Morken, J. P. *Science* **1998**, *280*, 267−270.
(50) Enjalbal, C.; Martinez, J.; Aubagnac, J. L. *Mass Spectrom. Rev.* **2000**, *19*, 139−161.
(51) Gorlach, E.; Richmond, R.; Lewis, I. *Anal. Chem.* **1998**, *70*, 3227−3234.
(52) vanBreemen, R. B.; Huang, C. R.; Nikolic, D.; Woodbury, C. P.; Zhao, Y. Z.; Venton, D. L. *Anal. Chem.* **1997**, *69*, 2159−2164.
(53) Senkan, S. M. *Nature* **1998**, *394*, 350−353.
(54) Senkan, S.; Krantz, K.; Ozturk, S.; Zengin, V.; Onal, I. *Angew. Chem., Int. Ed.* **1999**, *38*, 2794−2799.
(55) Senkan, S. M.; Ozturk, S. *Angew. Chem., Int. Ed.* **1999**, *38*, 791−795.
(56) Snively, C. M.; Oskarsdottir, G.; Lauterbach, J. *Angew. Chem., Int. Ed.* **2001**, *40*, 3028−3030.
(57) Snively, C. M.; Oskarsdottir, G.; Lauterbach, J. *J. Comb. Chem.* **2000**, *2*, 243−245.
(58) Lavastre, O.; Morken, J. P. *Angew. Chem., Int. Ed.* **1999**, *38*, 3163−3165.
(59) Cooper, A. C.; McAlexander, L. H.; Lee, D. H.; Torres, M. T.; Crabtree, R. H. *J. Am. Chem. Soc.* **1998**, *120*, 9971−9972.
(60) Crabtree, R. H. *Chem. Commun.* **1999**, 1611−1616.
(61) Jayaraman, S.; Hillier, A. C. *Langmuir* **2001**, *17*, 7857−7864.
(62) Shah, B. C.; Hillier, A. C. *J. Electrochem. Soc* **2000**, *147*, 3043−3048.
(63) Zhou, J.; Zu, Y.; Bard, A. J. *J. Electroanal. Chem.* **2000**, *491*, 22−29.
(64) Jambunathan, K.; Shah, B. C.; Hudson, J. L.; Hillier, A. C. *J. Electroanal. Chem.* **2001**, *500*, 279−289.
(65) Jambunathan, K.; Hillier, A. C. *J. Electroanal. Chem.* **2002**, *524−525*, 144−156.
(66) Kwak, J.; Bard, A. J. *Anal. Chem.* **1989**, *61*, 1794−99.
(67) Bard, A. J.; Fan, F.-R. F.; Pierce, D. T.; Unwin, P. R.; Wipf, D. O.; Zhou, F. *Science* **1991**, *254*, 68−74.
(68) Lee, C.; Miller, C. J.; Bard, A. J. *Anal. Chem.* **1991**, *63*, 78−83.
(69) Christensen, P. A.; Hamnett, A. *Techniques and Mechanisms in Electrochemistry*, 1st ed.; Blackie Academic & Professional: London, New York, 1994.
(70) Hadzi-Jordanov, S.; Angerstein-Kozlowska, H.; Vukovic, M.; Conway, B. E. *J. Phys. Chem.* **1977**, *81*, 2271−2279.
(71) Liu, R.; Iddir, H.; Fan, Q.; Hou, G.; Bo, A.; Ley, K. L.; Smotkin, E. S.; Sung, Y.-E.; Kim, H.; Thomas, S.; Wieckowski, A. *J. Phys. Chem. B* **2000**, *104*, 3518−3531.
(72) Green, C. L.; Kucernak, A. *J. Phys. Chem. B* **2002**, *106*, 1036−1047.
(73) Green, C. L.; Kucernak, A. *J. Phys. Chem. B* **2002**, *106*, 11446−11456.
(74) Bard, A. J.; Mirkin, M. V.; Unwin, P. R.; Wipf, D. O. *J. Phys. Chem.* **1992**, *96*, 1861−1868.
(75) Watanabe, M.; Motoo, S. *Electroanal. Chem. Interfac. Electrochem.* **1975**, *60*, 275−283.
(76) Koper, M. T. M.; Lukkien, J. J.; Jansen, A. P. J.; van Santen, R. A. *J. Phys. Chem. B* **1999**, *103*, 5522−5529.
(77) Koper, M. T. M.; Shubina, T. E.; van Santen, R. A. *J. Phys. Chem. B* **2002**, *106*, 686−692.
(78) Wang, K.; Gasteiger, H. A.; Markovic, N. M.; Ross, P. N. *Electrochim. Acta* **1996**, *41*, 2587−2593.
(79) Jarvi, T. D.; Stuve, E. M. *Electrocatalysis*, 1st ed.; Wiley-VCH: New York, 1998.
(80) Lu, G. Q.; Chrzanowski, W.; Wieckowski, A. *J. Phys. Chem. B* **2000**, *104*, 5566−5572.
(81) Lin, W. F.; Zei, M. S.; Eiswirth, M.; Ertl, G.; Iwasita, T.; Vielstich, W. *J. Phys. Chem. B* **1999**, *103*, 6968−6977.
(82) Villegas, I.; Weaver, M. J. *J. Chem. Phys.* **1994**, *101*, 1648.
(83) Lucas, C. A.; Markovic, N. M.; Ross, P. N. *Surf. Sci.* **1999**, *425*, L381−L386.
(84) Richarz, F.; Wohlmann, B.; Vogel, U.; Hoffschulz, H.; Wandelt, K. *Surf. Sci.* **1995**, *335*, 361−371.
(85) Frelink, T.; Visscher, W.; vanVeen, J. A. R. *Langmuir* **1996**, *12*, 3702−3708.
(86) Gasteiger, H. A.; Markovic, N.; Ross, P. N.; Cairns, E. J. *J. Phys. Chem.* **1994**, *98*, 617−625.
(87) Ianniello, R.; Schmidt, V. M.; Stimming, U.; Stumper, J.; Wallau, A. *Electrochim. Acta* **1994**, *39*, 1863−1869.
(88) Crown, A.; Kim, H.; Lu, G. Q.; de Moraes, I. R.; Rice, C.; Wieckowski, A. *J. New Mater. Electrochem. Syst.* **2000**, *3*, 275−284.
(89) Bonnemann, H.; Brinkmann, R.; Britz, P.; Endruschat, U.; Mortel, R.; Paulus, U. A.; Feldmeyer, G. J.; Schmidt, T. J.; Gasteiger, H. A.; Behm, R. J. *J. New Mater. Electrochem. Syst.* **2000**, *3*, 199−206.
(90) Pourbaix, M. *Atlas of Electrochemical Equilibria in Aqueous Solutions*, 2nd ed.; National Association of Corrosion Engineers: Houston, TX, 1974.
(91) Samjeske, G.; Wang, H.; Loffler, T.; Baltruschat, H. *Electrochim. Acta* **2002**, *47*, 3681−3692.
(92) Kabbabi, A.; Faure, R.; Durand, R.; Beden, B.; Hahn, F.; Leger, J. M.; Lamy, C. *J. Electroanal. Chem.* **1998**, *444*, 41−53.